DISLOCATIONS IN CRYSTALS

Keshra Sangwal
LUBLIN UNIVERSITY OF TECHNOLOGY

I. Dislocations: basic concepts
II. Sources of dislocations and their multiplication
III. Mechanical properties of crystals
IV. Dislocations and crystal growth
V. Morphology of crystals

I. Dislocations: basic concepts

Geometry and general features of dislocations

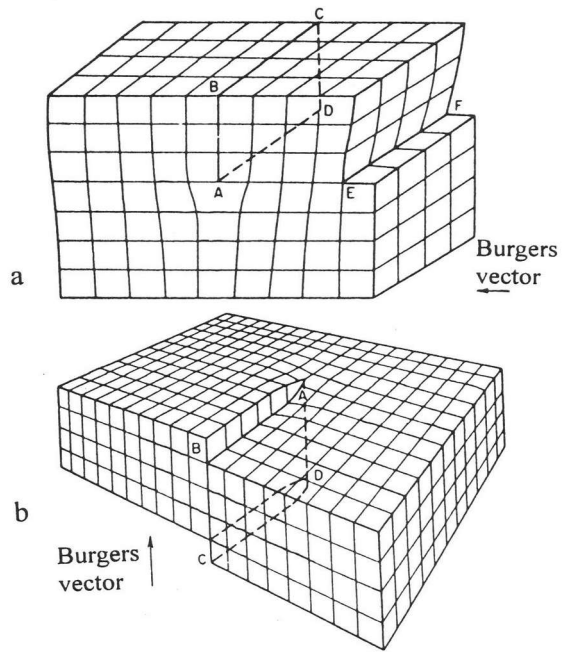

Fig. 1.2. Dislocations in a simple cubic lattice: (a) edge dislocation and (b) screw dislocation.

edge

screw

$K = 1-\nu$,
ν - Poisson coefficient ≈ 0.3

$K = 1$

Elastic deformation (strain) energy of dislocation (per unit length):

$$E_{el} = \frac{Gb^2}{4\pi K}\ln\left(\frac{r}{r_0}\right)$$ (6-10 eV)

G – shear modulus ($G \approx 10^{11}$ N/m^2),
b – Burgers vector ($2.5\cdot10^{-10}$ m),
r_0 – distance beyond which elasticity theory applies. Usually, it is assumed that $r/r_0 \approx 10^4$.

Core energy of a dislocation

$E_{core} < 3R_G T_m$. $E_{core}/E_{el} < 1/10$

Line tension T of a dislocation, i.e. increase in energy per unit length

$T \approx Gb^2$

Thus, one finds :
- E_{disl} mainly comes from E_{el} ($\approx Gb^2$);
  E_{disl}(screw) $\approx 0.7E_{disl}$(edge).
- E_{disl} is about $10E_V$, E_V – energy for creating a vacancy.

Burgers vector and Burgers circuit

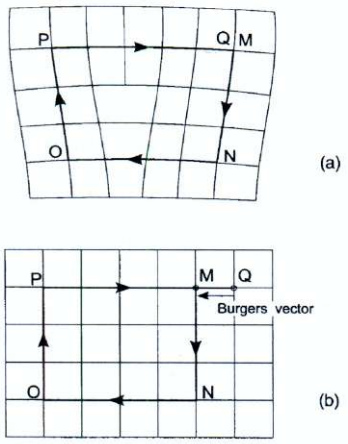

Figure 1.19 (a) Burgers circuit round an edge dislocation with positive line sense into the paper (see text), (b) the same circuit in a perfect crystal; the closure failure is the Burgers vector.

b ⊥ DL

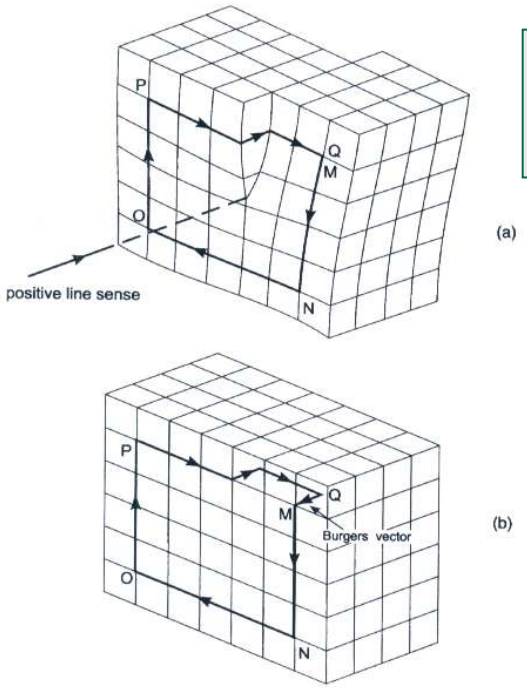

Dislocation Line – DL

b ∥ DL

Figure 1.20 (a) Burgers circuit round a screw dislocation with positive line sense in the direction shown; (b) the same circuit in a perfect crystal; the closure failure is the Burgers vector.

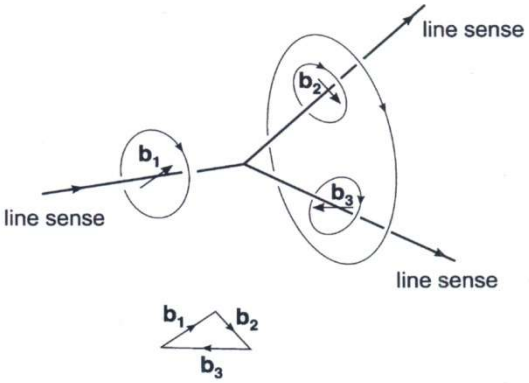

Figure 1.21 Three dislocations forming a node.

$$\mathbf{b}_1 = \mathbf{b}_2 + \mathbf{b}_3$$

$$E_1 > E_2 + E_3$$

b – unit vector

Grain boundaries

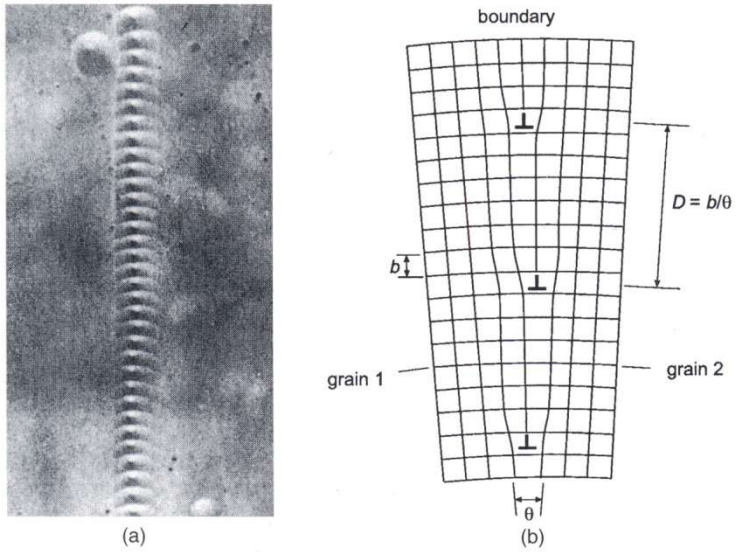

Figure 2.3 (a) A row of etch pits formed at the boundary between two germanium crystals. The etch pits are uniformly spaced. (b) Diagrammatic representation of the arrangement of dislocations in the boundary revealed by the etch pits in (a). This is a symmetrical pure tilt boundary which consists of a vertical array of edge dislocations with parallel Burgers vectors of the same sign. (After Vogel, Pfann, Corey and Thomas, *Physical Review* **90**, 489, 1953.)

General relation

$$\frac{b}{D} = 2\sin\frac{\theta}{2}$$

For small angles:
$\theta = b/D$.

Tilt boundaries:
Small- or Low-angle
Large-angle

Twist boundary

Boundaries formed by dislocations:
- edge,
- screw.

Stacking faults and partial vectors

hcp and fcc structures

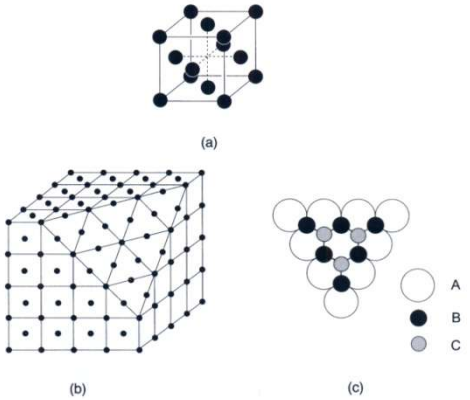

Figure 1.7 Face-centred cubic structure: (a) unit cell, (b) arrangement of atoms in a (111) close-packed plane, (c) stacking sequence of {111} planes.

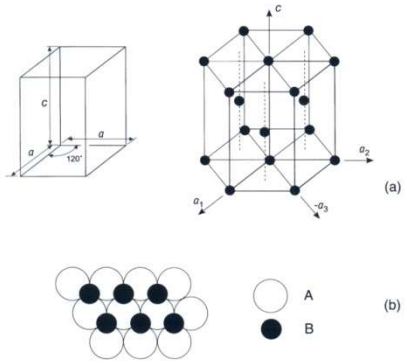

Figure 1.8 Close-packed hexagonal structure: (a) the unit cell of the lattice and the hexagonal cell showing the arrangement of atoms, (b) *ABAB*... stacking sequence of the atomic planes perpendicular to the *c* axis.

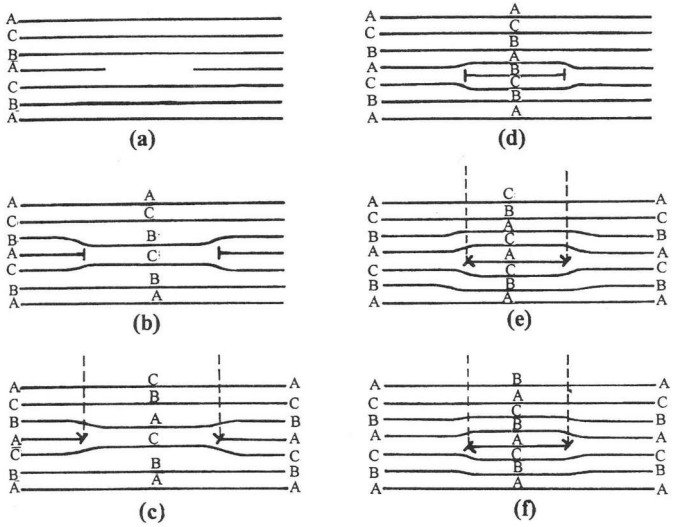

Fig. 1.13. Formation of Frank loops by the precipitation of (a–c) vacancies and (d–f) interstitials in disc-shaped aggregates on the (111) plane of the fcc structure: (a) vacancy disc, (b) Frank loop with $b = \frac{1}{3}[111]$, (c) sweeping of Frank loop by a Shockley partial and its transformation into a perfect loop with $b = \frac{1}{2}[110]$, (d) interstitial disc forming a Frank loop with $b = \frac{1}{3}[111]$, (e) sweeping of the Frank loop by one Shockley partial, and (f) sweeping of the loop by a second Shockley partial producing a perfect loop. Note that (d) contains an extrinsic fault while (e) contains an intrinsic fault. After Amelinckx (1979).

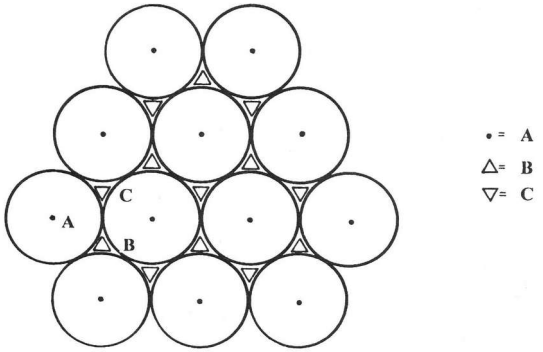

Fig. 1.10. Arrangement of a single closest-packed layer of atoms with their centres at points A and two types of hollows B and C above the layer.

Partial dislocations and partial vectors

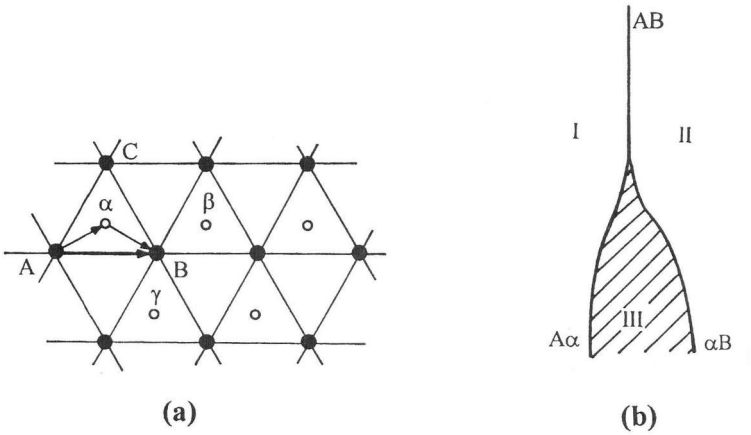

Fig. 1.11. (a) Possible Burgers vectors in the close-packed structure. Filled circles denote atoms in close-packed plane while open circles atoms in succeeding close-packed planes. (b) Splitting of a complete dislocation AB into partials $A\alpha$ and αB at the point O. After Kosevich (1979).

Metals: Mg, Cd, Zn
Structure: hcp
Close-packed plane: (1000)
Close-packed direction: $<11\bar{2}0>$
Unit lattice vector: $(1/3)<11\bar{2}0>$

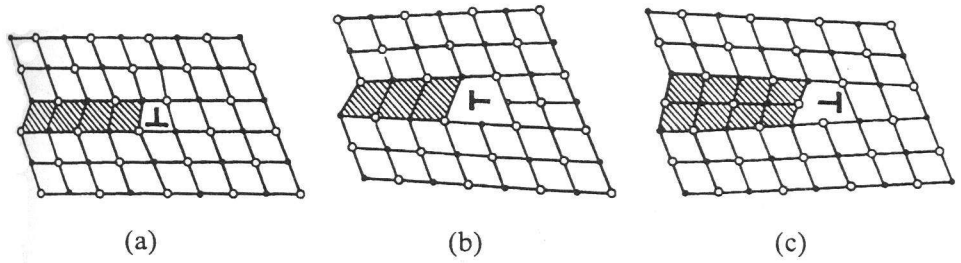

Fig. 1.12. Partial dislocations in the fcc structure: (a) Shockley dislocation, (b) negative Frank dislocation, and (c) positive Frank dislocation. The shaded area represents a stacking fault.

Some methods for revealing dislocations

- Spiral growth
- Chemical etching
- Thermal etching
- Decoration technique
- Topographic methods
- Photoelastic method
- Electron microscopy

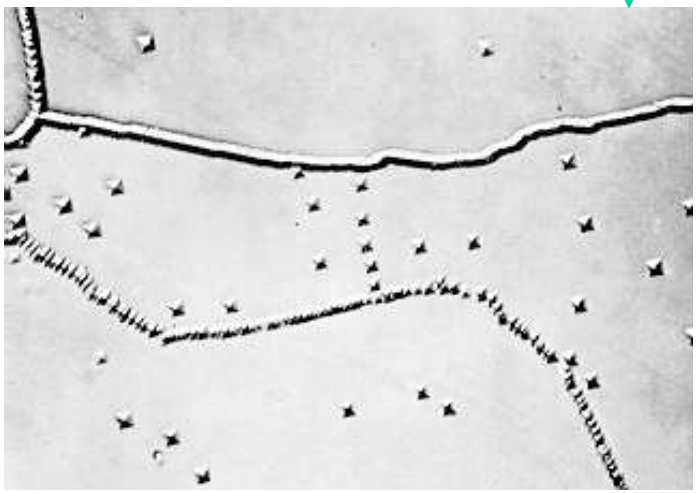

(100) LiF; Water + Fe(III) ions
(Gilnan & Johnston, 1957)

Macromolecular crystals

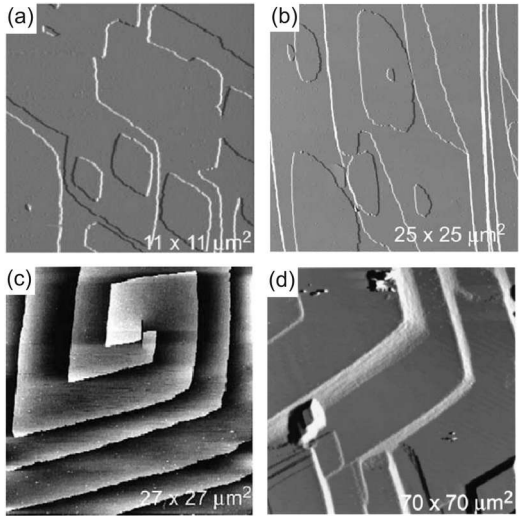

A. McPherson et al., J. Struct. Biol. 142 (2003) 32.

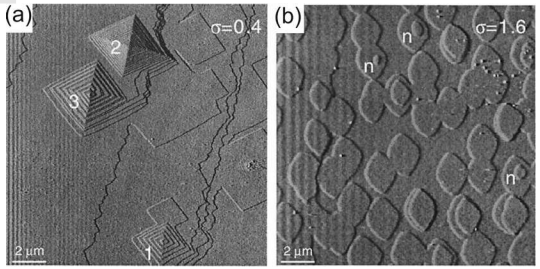

Calcite

H.H. Tenh et al., Geochim. Cosmochim ActaJ. 64 (2000) 2255.

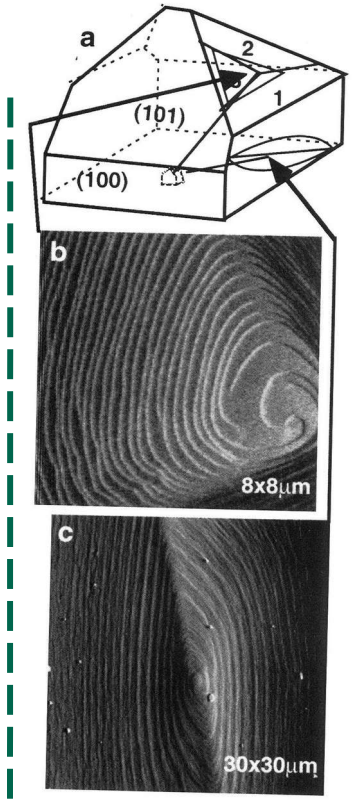

Figure 6. Example of KDP crystal surfaces preserved by pulling through hexane. (a) shows schematic of crystal structure. (b and c) Growth hillocks on the (b) {101} and (c) {100} face generated by dislocations emanating from the seed crystal interface.

J.J. De Yoreo et al., in: Advances in Crystal Growth, Eds. K. Sato et al., Elsevier, 2001, p. 361-380.

Dislocation density: ρ
dislocation lines intersecting observation plane per cm².

Literature:
- K. Sangwal, Etching of Crystals, North-Holland, Amsterdam (1987).
- D. Hull, D.J. Bacon, Introduction to Dislocations, 4th edition, Butterworth-Heinemann, Oxford (2001).

Examples of dislocations

Lefaucheux et al., JCG 67 (1984) 541.

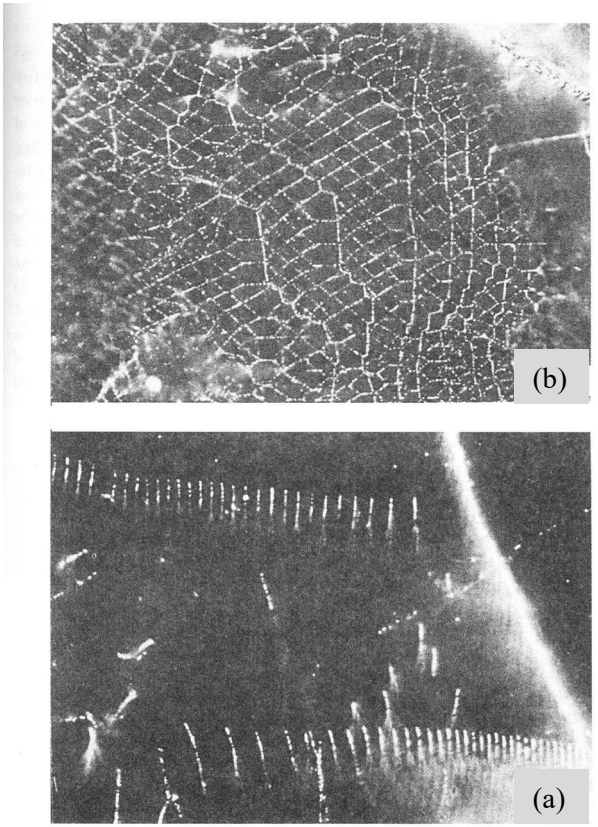

Fig. 1.19. (a) Symmetrical tilt boundaries and (b) a square network containing zigzag singularities observed in decorated KCl crystals by optical microscopy. From Amelinckx (1979).

Decoration

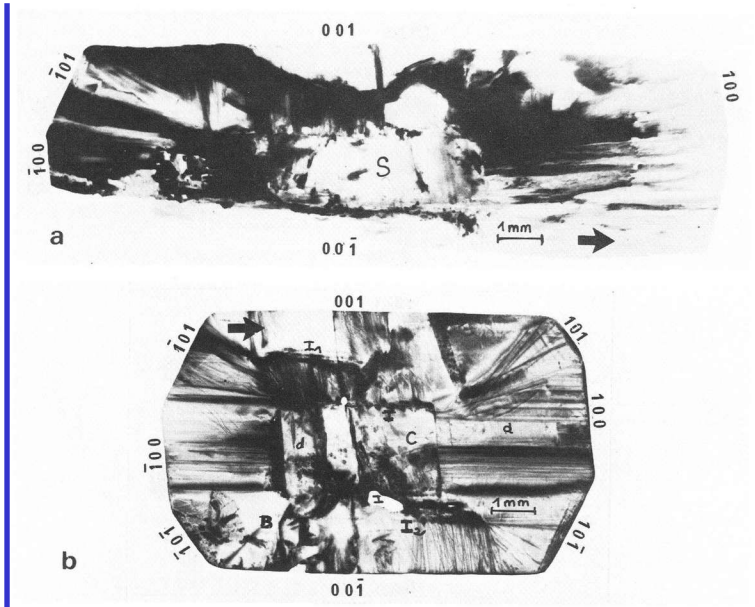

Fig. 1. (a) Topograph of a (010) slice cut out of a KBC crystal grown at $T_G = 29.2\,^\circ C$; growth duration 17 h; ref. 002; MoKα. (b) Topograph of a (010) slice cut out of a KBC crystal grown at $T_G = 56\,^\circ C$; growth duration 5 h; ref. 002; MoKα.

X-ray topography

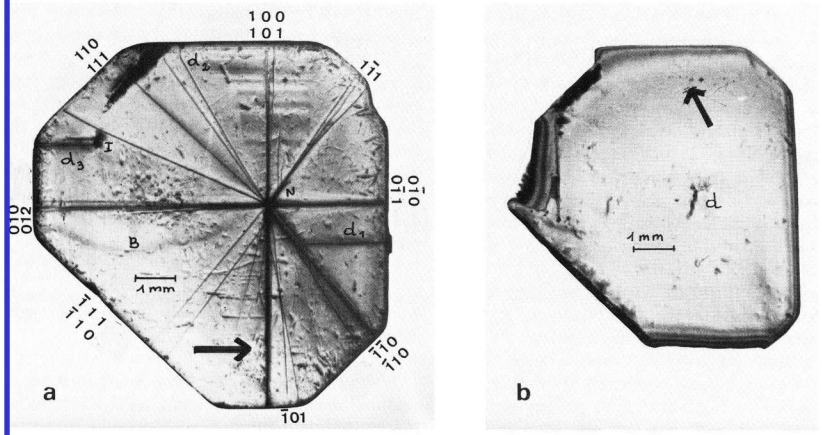

Fig. 6. Topographs of the two (010) slices cut out of an as grown KBC crystal obtained at 90 °C: (a) lower slice, ref. 200; (b) upper slice, ref. $1\bar{2}0$; MoKα.

II. Sources of dislocations and their multiplication

Dislocations during growth

Mechanism I:
Step bunching and macrosteps

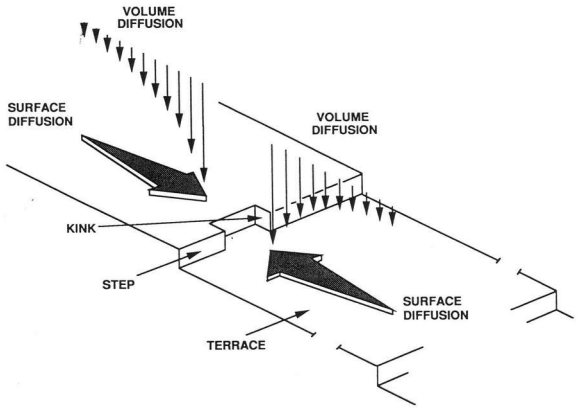

Figure 3.4 Important diffusional processes (volume and surface) affecting crystal growth. (Reproduced with permission from Rosenberger 1986.)

Impurities

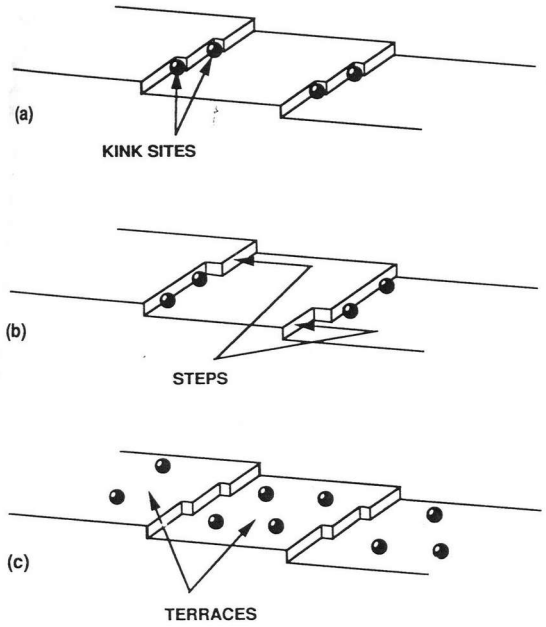

Figure 3.5 Key surface structures on an idealized crystal face: (a) kinks; (b) steps; and (c) terraces. Adsorbed impurities at each of these sites is illustrated. (Reproduced with permission from Mullin 1980.)

Volume diffusion

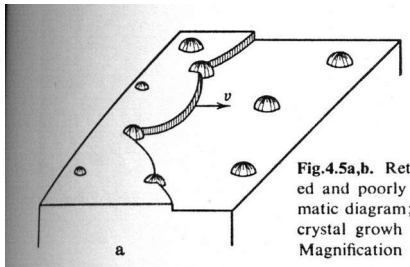

Fig.4.5a,b. Retardation of a step by strongly adsorbed and poorly trapped impurity particles. **(a)** Schematic diagram; **(b)** photo of the basal face of a SiC crystal growth from vapor, in reflected light [4.21] Magnification × 250

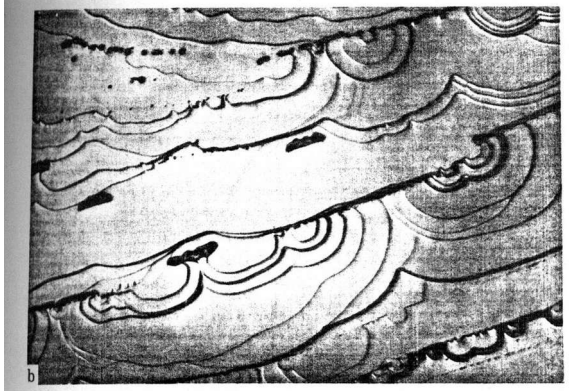

Trapping of mother liquor and impurity clusters

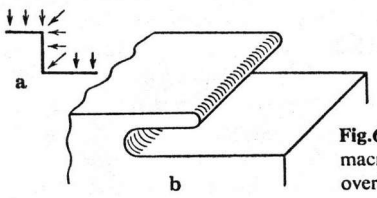

Fig.6.1a,b. Nonuniformity in the nutrition of a macrostep rise (**a**) and the resulting formation of an overhanging layer and a flat inclusion under it (**b**)

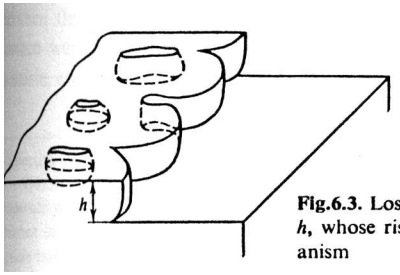

Fig.6.3. Loss of stability by a macrostep of thickness *h*, whose rise grows according to the normal mechanism

Inclusions

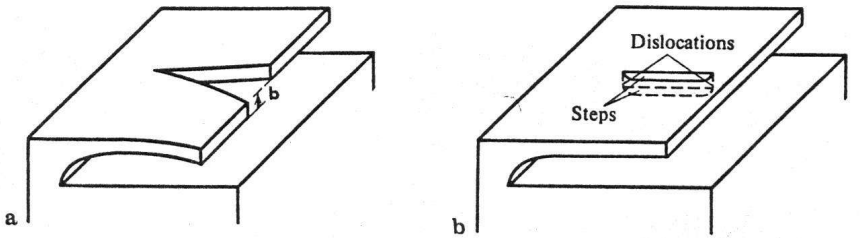

Fig.6.11. Reentrant angle on a thin overhanging layer (**a**) and its overgrowth with the formation of dislocations (**b**) according to the mechanism of Figs. 3.25, 26; ***b*** is the displacement Burgers vector

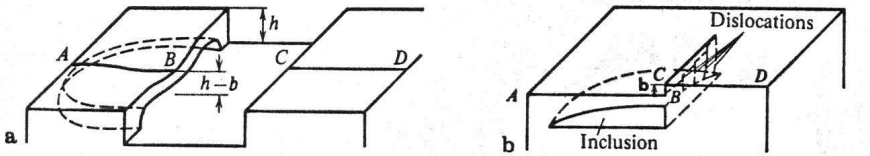

Fig.6.12a,b. Creation of dislocations accompanying the trapping of mother liquor. (**a**) Buckling of the overhanging layer; (**b**) closing up of the inclusion when macrosteps meet with forming dislocations (section on ABCD); *h* is the step height, and ***b*** the Burgers vector

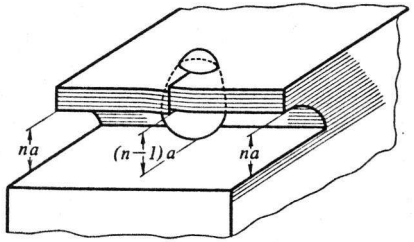

Fig.6.10. The formation of dislocations when a foreign macroparticle is trapped by a plate-like crystal or an overhanging layer. The two parts of the closed-up layer are shifted with respect to one another by the value of the interplanar distance [6.14]

Dislocations

Misfit dislocations

Epitaxy
- homo-epitaxy
- hetero-epitaxy

Mechanism II:

Mismatch between lattice parameters of substrate and growth layer

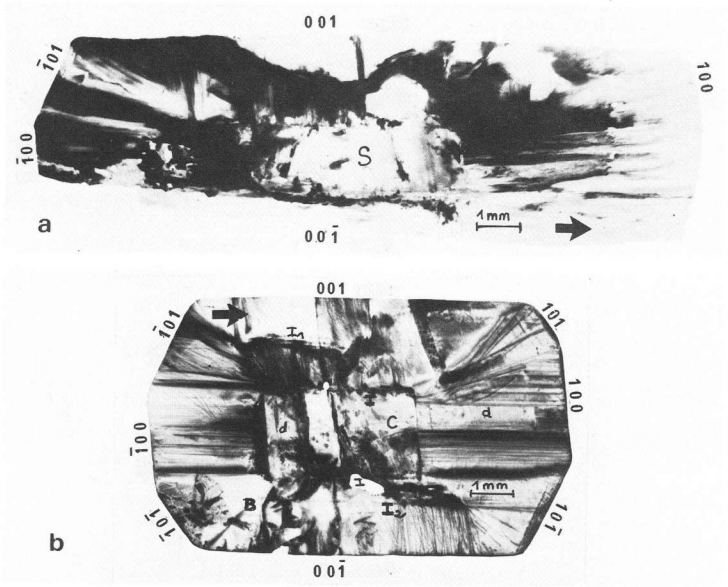

Fig. 1. (a) Topograph of a (010) slice cut out of a KBC crystal grown at $T_G = 29.2\,^{\circ}C$; growth duration 17 h; ref. 002; MoKα. (b) Topograph of a (010) slice cut out of a KBC crystal grown at $T_G = 56\,^{\circ}C$; growth duration 5 h; ref. 002; MoKα.

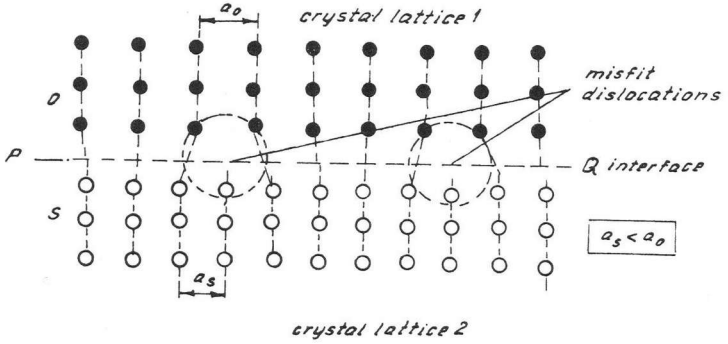

Figure 12.2. A pure misfit dislocation geometry of edge type at interface PQ of crystals O (overgrowth) and S (substrate), with lattice spacings a_O and a_S, respectively [12].

Linear density of misfit dislocations

$$\rho = \frac{a_2 - a_1}{a_1 a_2} \approx \frac{\Delta a}{a^2},$$

gdzie $a_1 \approx a_2 \approx a$.

Lefaucheux et al., JCG 67 (1984) 541.

Diffusion of vacancies and atoms

Mechanism III
Condensation of vacancies and interstitial atoms

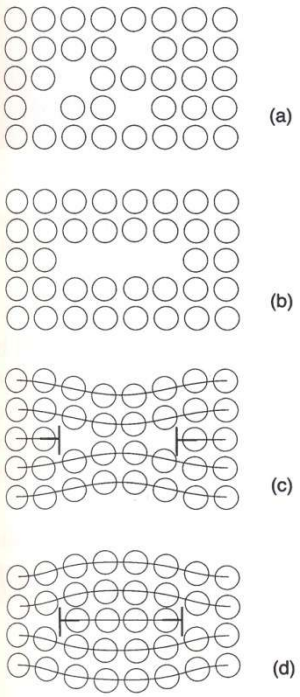

Figure 3.18 Formation of a prismatic dislocation loop. (a) Represents a crystal with a large non-equilibrium concentration of vacancies. In (b) the vacancies have collected on a close-packed plane and in (c) the disc has collapsed to form an edge dislocation loop. (d) Loop formed by a platelet of self-interstitial atoms.

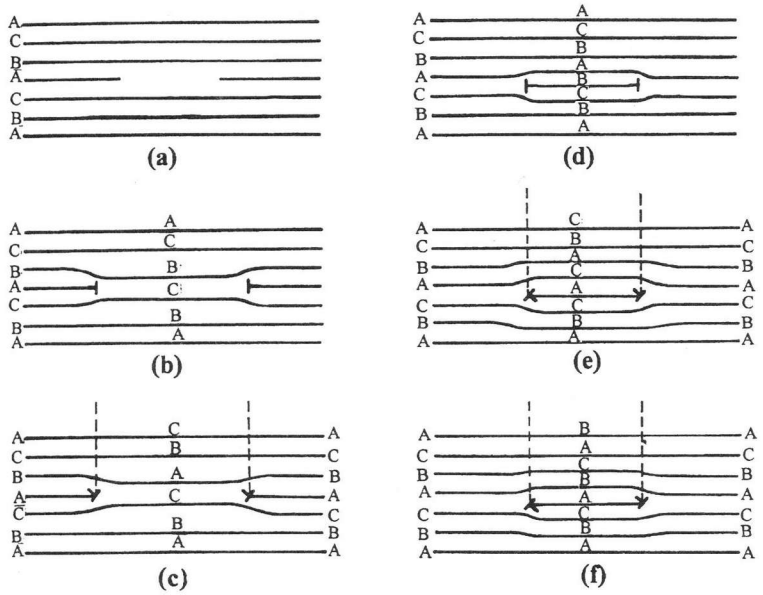

Fig. 1.13. Formation of Frank loops by the precipitation of (a–c) vacancies and (d–f) interstitials in disc-shaped aggregates on the (111) plane of the fcc structure: (a) vacancy disc, (b) Frank loop with $b = \frac{1}{3}[111]$, (c) sweeping of Frank loop by a Shockley partial and its transformation into a perfect loop with $b = \frac{1}{2}[110]$, (d) interstitial disc forming a Frank loop with $b = \frac{1}{3}[111]$, (e) sweeping of the Frank loop by one Shockley partial, and (f) sweeping of the loop by a second Shockley partial producing a perfect loop. Note that (d) contains an extrinsic fault while (e) contains an intrinsic fault. After Amelinckx (1979).

Nucleation and multiplication of dislocations

Mechanism IV

Internal stresses acting on a dislocation segment (Frank-Read source)

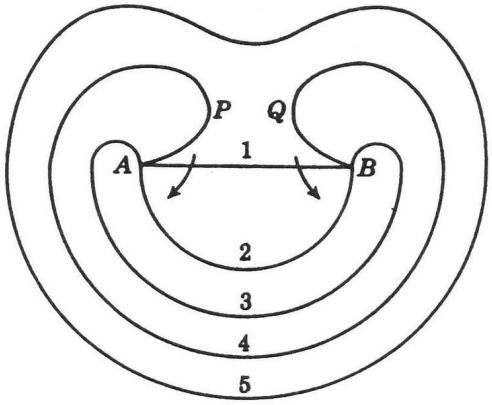

Fig. 1.5. Frank–Read mechanism of dislocation multiplication, showing different stages of formation of a dislocation loop from segment AB of a dislocation line.

Local stresses
(e.g. thermal stresses)
- nucleation center

Stresses acting in large area
- multiplication

III. Mechanical properties of crystals

Shear strength of single crystals

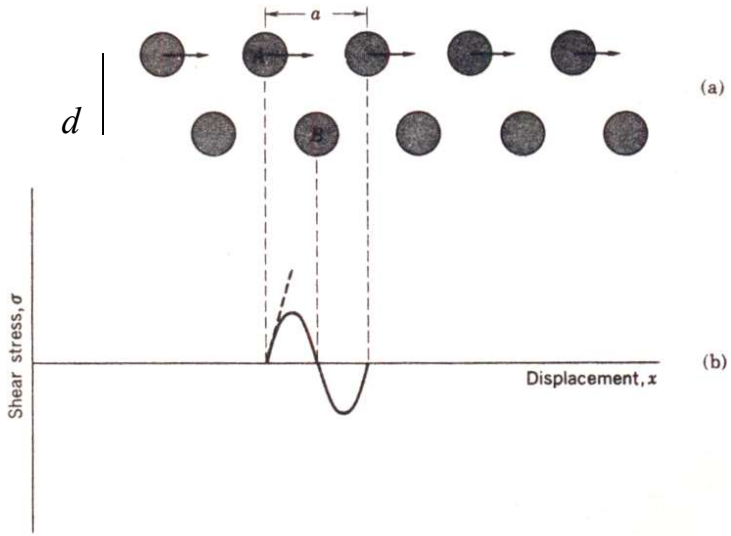

Figure 1 (a) Relative shear of two planes of atoms (shown in section) in a uniformly strained crystal; (b) shear stress as a function of the relative displacement of the planes from their equilibrium position. The heavy broken line drawn at the initial slope defines the shear modulus *G*.

For low elastic deformation, the acting shear stress

$$\sigma = Gx/d$$

In the entire deformation interval the shear stress σ is a periodic function of *a*, i.e.

$$\sigma = \frac{Ga}{2\pi d}\sin\left(\frac{2\pi x}{a}\right)$$

Critical value of shear stress

$$\sigma_c = \frac{Ga}{2\pi d}$$

Theoretically, for $d = a$:

$G/\sigma_c < 10$

Experiments show that for different crystals:

$G/\sigma_c = 10^2 - 10^4$.

Movement of dislocations

Concept of glide (slip)

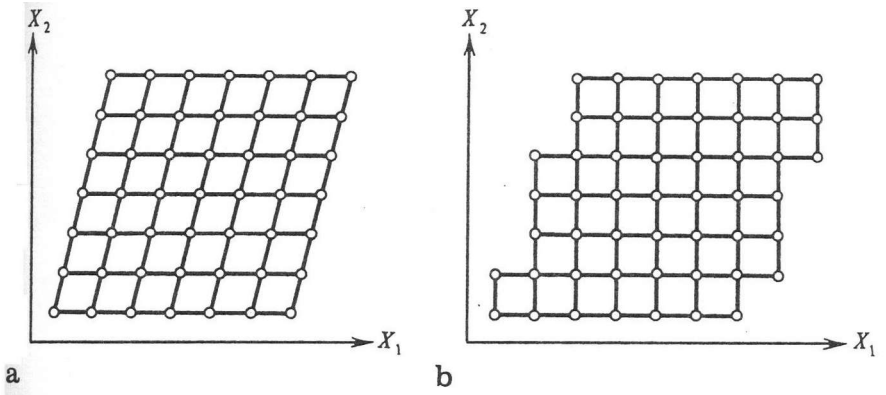

Fig. 3.2. Schematic illustration of (a) elastic and (b) plastic deformation of a tv

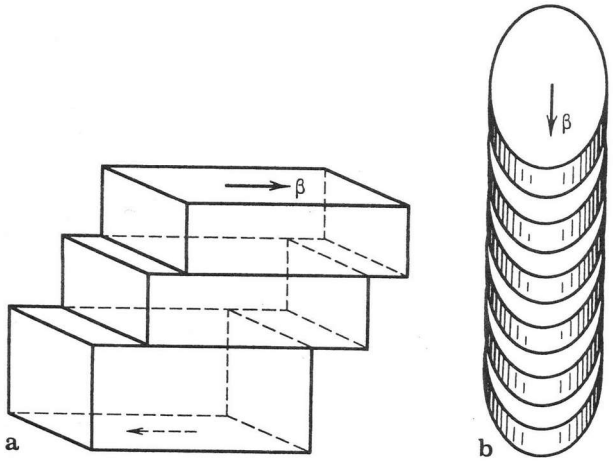

Fig. 3.1. Model of glide under shear stresses β in a specimen of (a) cubic and (b) cylindrical shape.

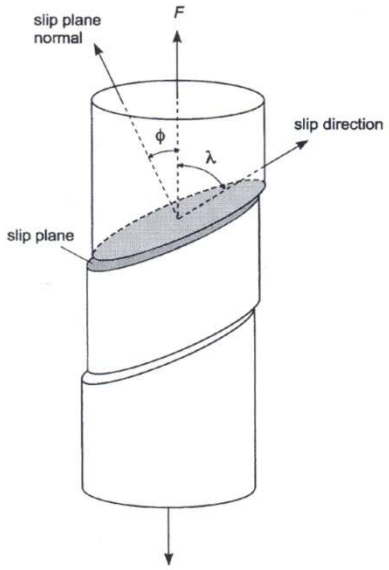

Figure 3.1 Illustration of the geometry of slip in crystalline materials. Note that $(\phi + \lambda) \neq 90°$ in general.

Tangential stress along slip direction (called shear stress):

$\tau = (F/A)\cos\phi\cos\lambda$.

Slip system: (100)[010].

Primary and secondary slip systems.

Slip and dislocations

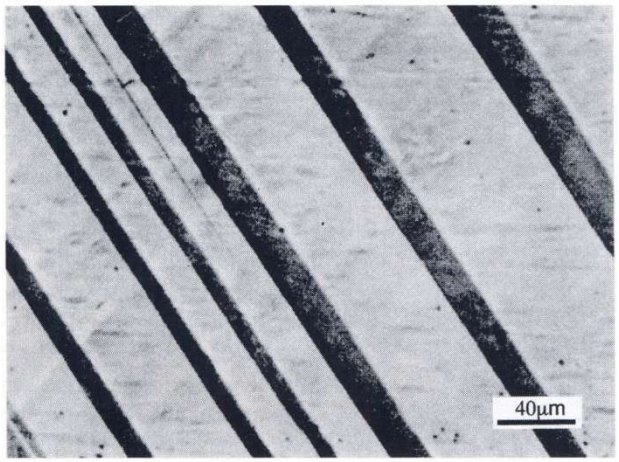

(a)

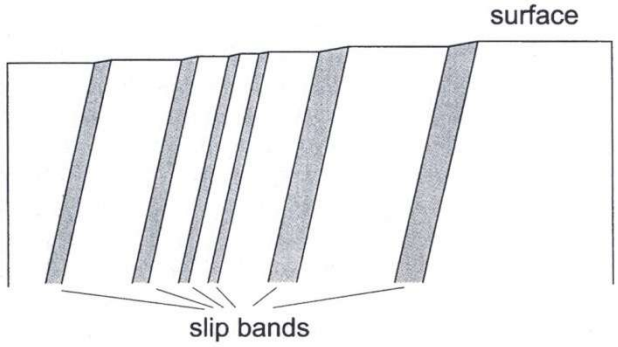

(b)

Figure 3.2 (a) Straight slip bands on a single crystal of 3.25 per cent silicon iron. (From Hull, *Proc. Roy. Soc.* **A274**, 5, 1963.) (b) Sketch of a section across the slip bands normal to surface shown in (a). Each band is made up of a large number of slip steps on closely spaced parallel slip planes.

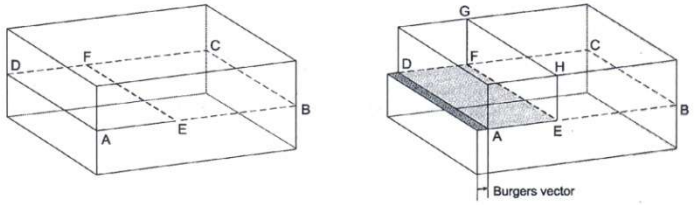

(a) (b)

Figure 3.3 Formation of a pure edge dislocation *FE*.

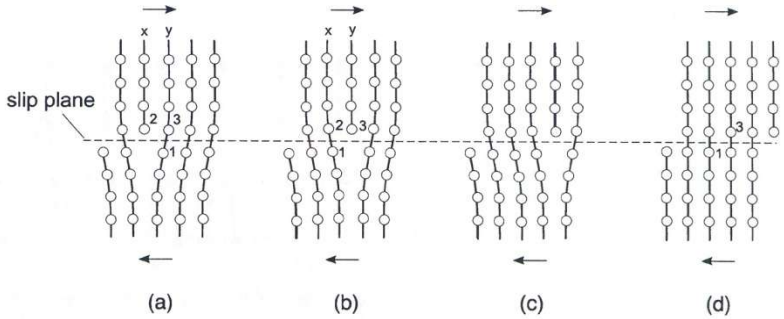

Figure 3.4 Movement of an edge dislocation: the arrows indicate the applied shear stress.

Slip occurs only in the case of edge dislocations

Cross slip

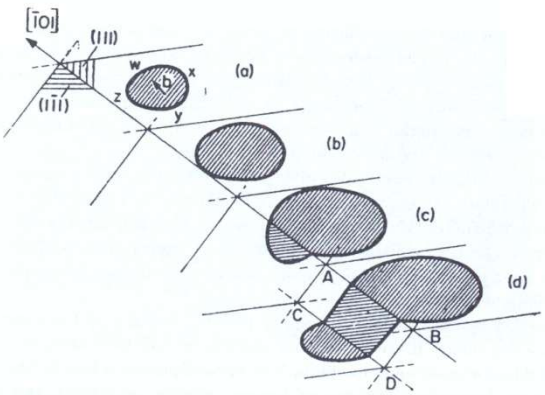

Fig. 1.4. Different stages of the expansion of a dislocation loop by cross slip in an fcc crystal. Close-packed planes (111) and (1$\bar{1}$1) have a common [$\bar{1}$01] direction. The screw component of the dislocation can glide freely on both planes. Stage (d) shows double cross slip. From Hull (1975).

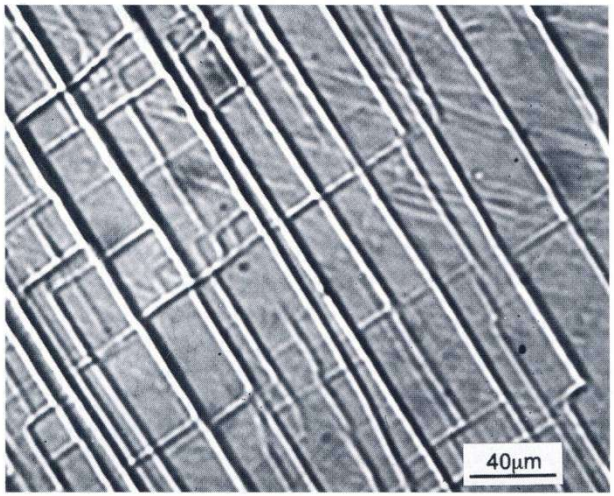

Figure 3.10 Cross slip on the polished surface of a single crystal of 3.25 per cent silicon iron.

In crystals of metals:
Close-packed planes like (111) have common direction like [$\bar{1}$01].

Screw dislocation components can glide freely on both planes. This process is very fast because it does not require any activation energy.

Dislocation climb

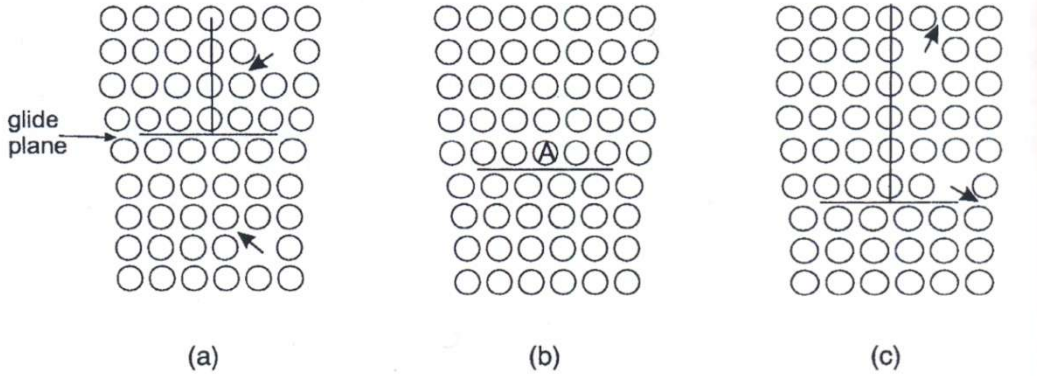

Figure 3.13 Positive and negative climb of an edge dislocation. In (b) the dislocation is centred on the row of atoms *A* normal to the plane of the diagram. If the vacancies in the lattice diffuse to the dislocation at *A* the dislocation will climb in a positive sense as in (a). If vacancies are generated at the dislocation line and then diffuse away the dislocation will climb in the negative sense as in (c).

Climb of dislocations can be both positive as well as negative. This is a slow process because it requires an activation energy for the movement of atoms from crystal interior to or from the plane of edge dislocations.

Characteristics of stress–strain curves

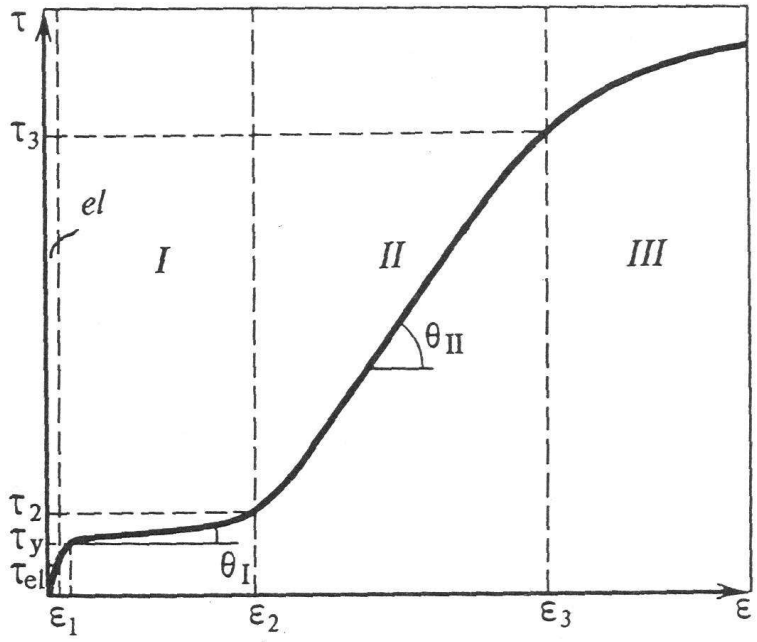

Fig. 3.14. Typical stress–strain curve for face-centred cubic single crystals.

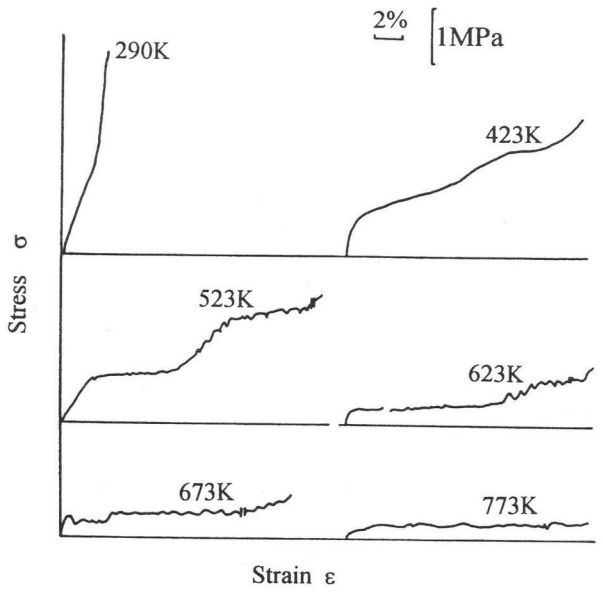

Fig. 3.15. Stress–strain curves of CsI crystals compressed at different temperatures. After Urusovskaya and Demchenko (1992).

θ - hardening coefficient or plasticity modulus

τ_y – yield point

θ_I – easy glide stage (small work hardening).

θ_{II} – fast linear hardening stage.

θ_{III} – strain softening or strain relaxation stage.

Barriers during dislocation glide

Motion of a dislocation through a crystal lattice encounters different barriers:
- periodiity of crystal lattice (Peierls-Nabarro barrier)
- stored and mobile dislocations (internal or background stresses)
- obstacles on slip planes (impurity atoms, other dislocations intersecting slip planes, boundaries of different types, precipitates, etc.

Peierls-Nabarro barrier

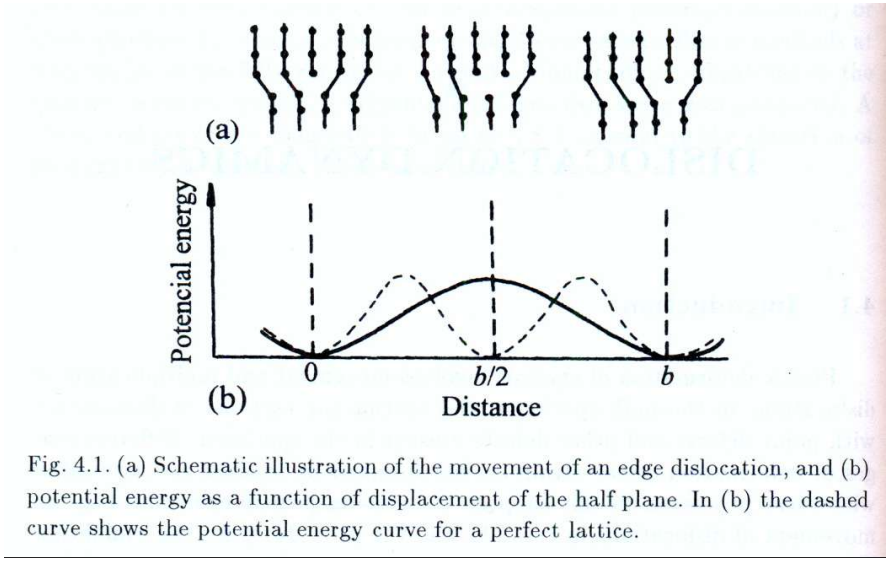

Fig. 4.1. (a) Schematic illustration of the movement of an edge dislocation, and (b) potential energy as a function of displacement of the half plane. In (b) the dashed curve shows the potential energy curve for a perfect lattice.

Energy per interatomic displacement is the applied stress τ_P (Peierls-Nabarro barrier)

Dependence of applied stress on displacement of a dislocation on its slip plane

$$\tau = \frac{Ga}{2\pi d}\sin\left(\frac{2\pi x}{a}\right)$$

Maximum value of stress τ (i.e. Peierls-Nabarro stress τ_P) has sinusoidal dependence

$$\tau_P = \frac{2G}{(1-\nu)}\exp\left(-\frac{2\pi w}{b}\right)$$

with the width of dislocation core $w = d/(1-\nu)$.

Note that τ_P is very sensitive to arrangement of atoms in dislocation core, i.e. d/b,
and taking $w = 3b$, for example, one has
$\tau_P \approx 10^{-3}G$,
in comparison with that for ideal crystals where
$\tau_P \approx 10^{-1}G$.

Table 4.1. Extrapolated values of experimental τ_P at 0 K for different types of crystals (Gil Sevillano 1993)

System	$(\tau_P)_0/G$
fcc metals and basal slip in hcp metals	$< 10^{-5}$
bcc metals, prismatic slip in hcp metals and slip in noncompact planes in fcc metals	5×10^{-3}
Ionic crystals: alkali halides	$10^{-2} - 2 \times 10^{-2}$
Ionic crystals: oxides	$10^{-2} - 3 \times 10^{-2}$
Covalent crystals	$2 \times 10^{-2} - 2 \times 10^{-2}$

Dislocation movement related to lattice resistance strongly depends on the activation energy for their lattice barrier and the activation distance.

Lattice resistance for metals is low, because:
- the activation energy is about 0.5 eV,
- their activation distance is about *b*/2.

Therefore, their flow stress τ_P strongly depends on temperature and strain rate.

Lattice resistance for covalent crystals is very high, because:
- the activation energy for their lattice barrier is as high as 5 eV.

Therefore, their flow stress τ_P strongly depends on temperature and strain rate.

Background internal stress due to dislocation forest:

$$\tau_B = \frac{Gb\rho^{1/2}}{4\pi(1-\nu)} = 0.1Gb\rho^{1/2}.$$

Dislocation density:
ρ - dislocation lines intersecting observation plane per cm^2.

Dislocation dynamics

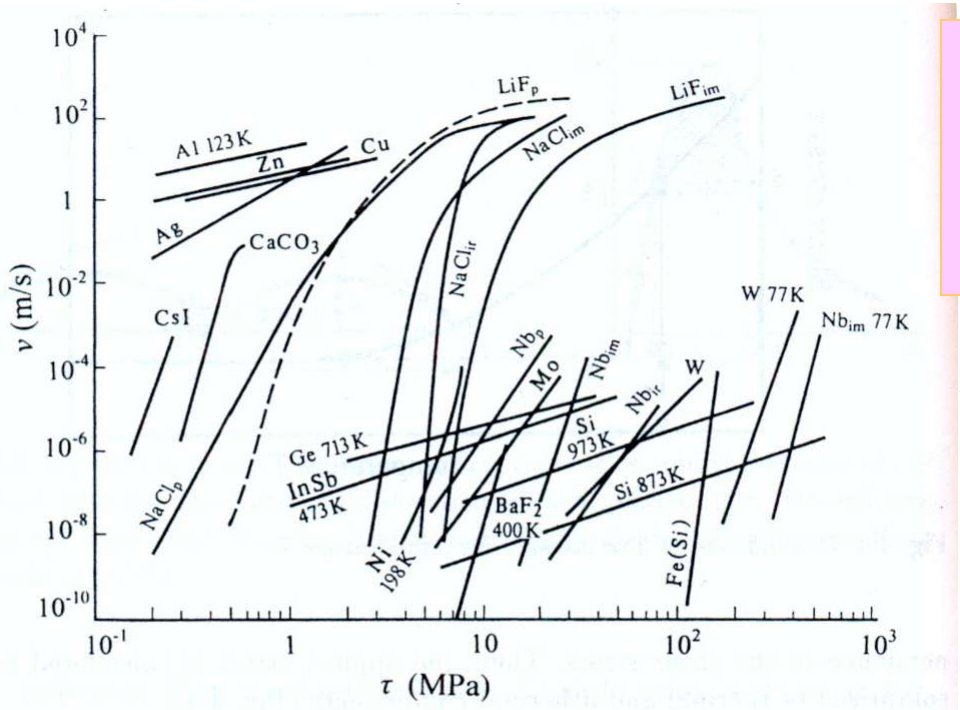

Fig. 4.5. Dislocation velocities as a function of applied stress in various crystals. Subscript "p" denotes pure crystals, subscript "im" crystals with impurities, and subscript "ir" irradiated. Where temperature is not indicated the data were obtained at room temperature. Compiled by Nadgornyi (see Roitburd 1972).

Dislocation velocity *v* depends on:
- crystal under observation,
- applied stress,
- temperature,
- impurities.

Arrhenius relation:

$$v = v_0 \exp\left(\frac{H(\tau)}{k_B T}\right)$$

Power-law relation:

$$v = v_0 \left(\frac{\tau}{\tau_0}\right)^n$$

H, v_0, τ_0 and *n* are constants.

J.J. Gilman, W.G. Johnston (1957-1965).
Most of the work in the area: up to 1980.

IV. Dislocations and crystal growth

J.J. De Yoreo et al., in: Advances in Crystal Growth, Eds. K. Sato et al., Elsevier, 2001, p. 361-380.

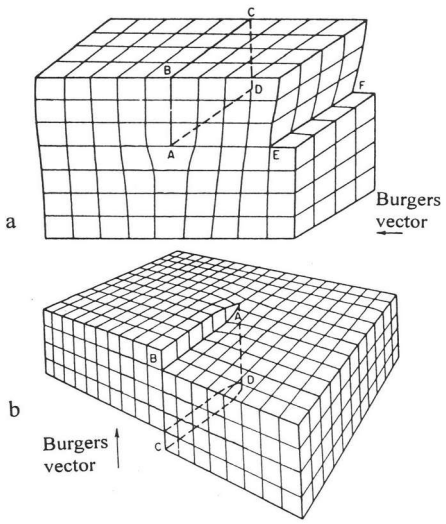

Fig. 1.2. Dislocations in a simple cubic lattice: (a) edge dislocation and (b) screw dislocation.

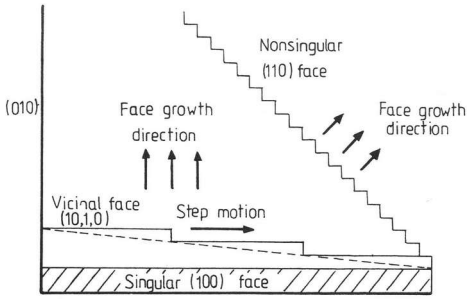

Figure 4.2. Cross-sectional view of the faces of different orientations of a simple cubic crystal [3].

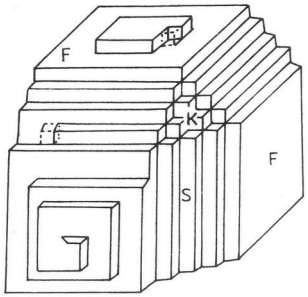

Figure 4.3. Classification of different types of faces of a simple cubic crystal according to the Periodic Bond Chains (PBC): F (flat), S (stepped) and K (kinked). From Ref. [6].

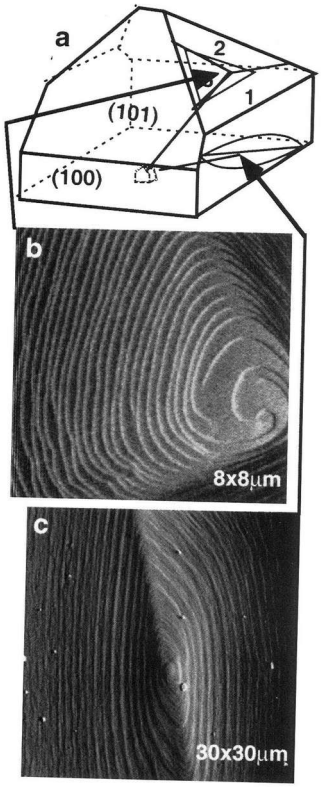

Figure 6. Example of KDP crystal surfaces preserved by pulling through hexane. (a) shows schematic of crystal structure. (b and c) Growth hillocks on the (b) {101} and (c) {100} face generated by dislocations emanating from the seed crystal interface.

Dislocation geometry

Growth mechanism

Growth surfaces

V. Morphology of crystals

Stability, metastability and unstability of media

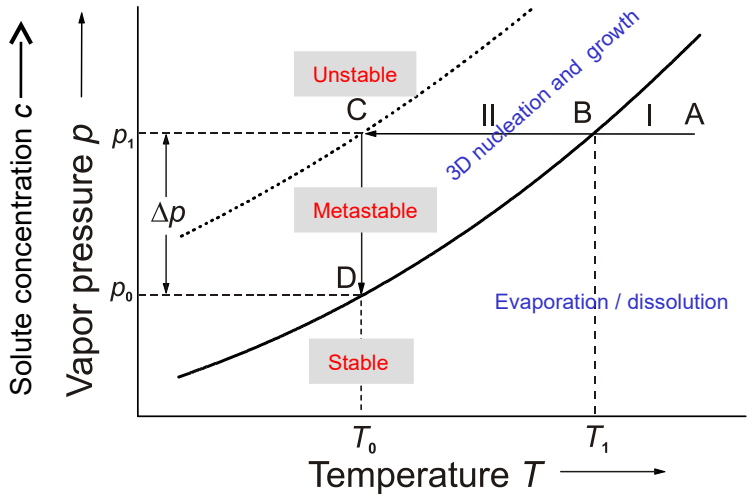

Schematic illustration of the dependence of vapor pressure *p* of a system on temperature. Solid curve shows the state when vapor phase I is in equilibrium with solid phase II, while dotted curve shows the upper limit of the metastable zone when precipitation of phase II occurs in the system. .

Crystal morphology (appearance)

- Overall morphology (macromorphology)
  Equilibrium and growth morphologies
- Surface morphology (micromorphology)

Growth habit of crystals

For examination of surface morphology of crystals by different techniques, surface cleanliness is very important.

Growth and dissolution/evaporation occur at crystal-medium interface, but the interface may be smooth or rough depending on the available supersaturation

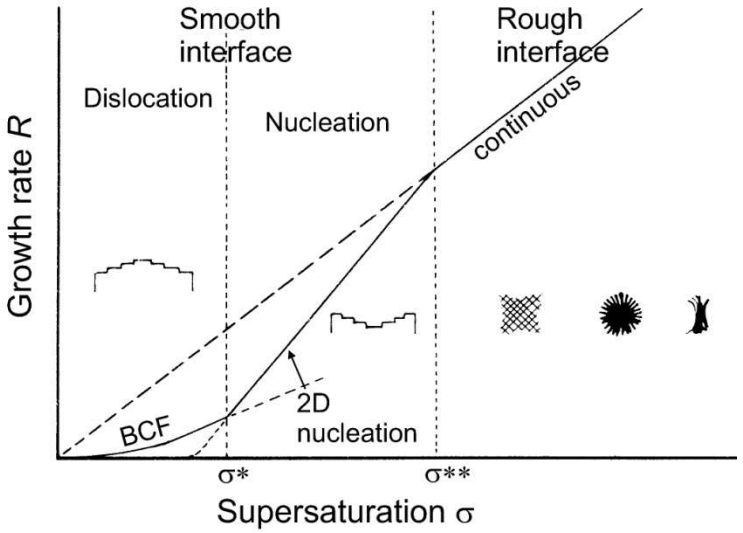

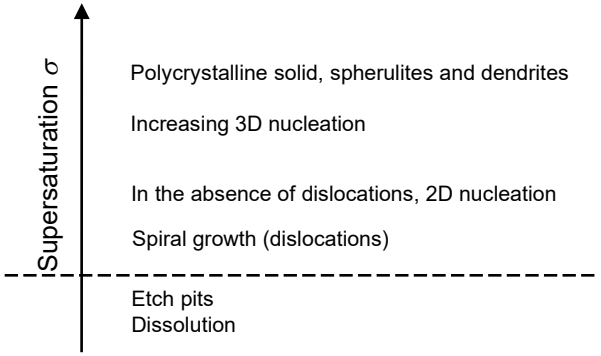

Schematic representation of the dependence of growth rate *R* on supersaturation σ for different growth mechanisms. After I. Sunagawa (1981). Bull. Mineral. 104 (1981) 81.

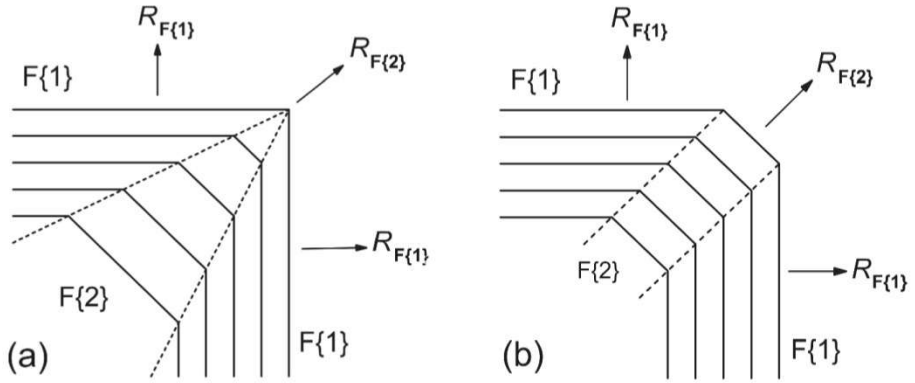

Schematic illustration of the difference in the development of F{1} and F{2} faces lying in the same zone in terms of their relative displacement rates under different growth conditions, leading to the (a) elimination and (b) persistence of F{2} face in the growth habit: (a) $R_{F\{1\}} < R_{F\{2\}}$ and (b) $R_{F\{1\}} > R_{F\{2\}}$.

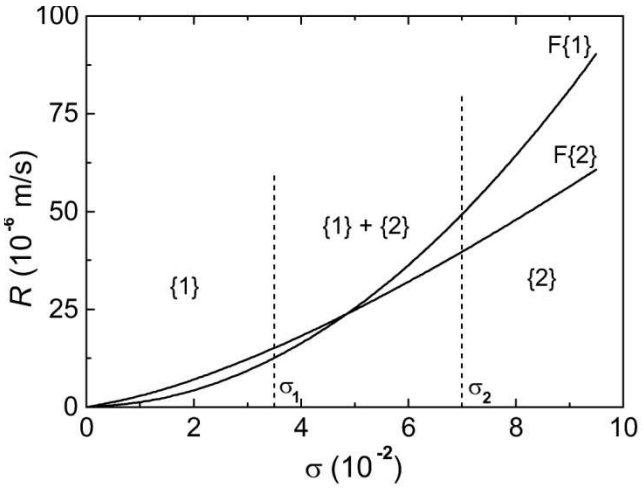

Growth morphology of a crystal composed of F{1} and F{2} faces in relation to supersaturation. Polyhedra {1} and {2} composed of F{1} and F{2} faces are formed at low and high supersaturations, respectively.

Literature

D. Hull, Introduction to Dislocations, Pergamon, Oxford (1975);

D. Hull, D.J. Bacon, Introduction to Dislocations, 4th edition, Butterworth-Heinemann, Oxford (2001).

C. Kittel, Introduction to Solid State Physics, 5th edition, Wiley, N.Y. (1976); and later editions.

A.A. Urusovskaya, K. Sangwal, Mechanical Properties of Crystalline and Noncrystalline Solids, Politechnika Lubelska, Lublin (2001).

A.A. Chernov (Editor), Modern Crystallography: Crystal Growth, Springer, Berlin (1984).

K. Sangwal, R. Rodriguez-Clemente, Surface Morphology of Crystalline Solids, Trans Tech, Zurich (1991).

I. Sunagawa (Editor), Morphology of Crystals. Terrapub, Tokyo (1987).

I. Sunagawa. Crystals: Growth, Morphology and Perfection, Cambridge University Press (2005).

Acknowledgement:

Krzysztof Zabielski for scan of several figures used here.